

Volumetric Super-Resolution of Multispectral Data

Vildan Atalay Aydin and Hassan Foroosh

Abstract

Most multispectral remote sensors (e.g. QuickBird, IKONOS, and Landsat 7 ETM+) provide low-spatial high-spectral resolution multispectral (MS) or high-spatial low-spectral resolution panchromatic (PAN) images, separately. In order to reconstruct a high-spatial/high-spectral resolution multispectral image volume, either the information in MS and PAN images are fused (i.e. pansharpening) or super-resolution reconstruction (SRR) is used with only MS images captured on different dates. Existing methods do not utilize temporal information of MS and high spatial resolution of PAN images together to improve the resolution. In this paper, we propose a multiframe SRR algorithm using pansharpened MS images, taking advantage of both temporal and spatial information available in multispectral imagery, in order to exceed spatial resolution of given PAN images. We first apply pansharpening to a set of multispectral images and their corresponding PAN images captured on different dates. Then, we use the pansharpened multispectral images as input to the proposed wavelet-based multiframe SRR method to yield full volumetric SRR. The proposed SRR method is obtained by deriving the subband relations between multitemporal MS volumes. We demonstrate the results on Landsat 7 ETM+ images comparing our method to conventional techniques.

Index Terms

Volumetric Multispectral Super-resolution, Discrete Wavelet Transforms Haar Domain Subband Relations

I. INTRODUCTION

Super-resolution and image restoration methods [33]–[35], [49], [78], [105], [119]–[121], [123]–[129], [132], [133], [135] have a wide-range of applications in various areas of imaging and computer vision, such as self-localization [90], [91], [94], [96]–[98], image annotation [151]–[156], surveillance [11], [15], [16], [81]–[83], [86]–[89], [95], [145], [147], [148], [150], action recognition [10], [12]–[14], [17], [18], [38], [137]–[142], [146], [149], object tracking [109]–[111], [134], [144], shape description and object recognition [1]–[3], [39]–[41], [56], [59], [106], [113], [164], scene modeling [1]–[3], [39]–[41], [56], [59], [106], [113], [164], image-based rendering [4], [5], [23], [29], [47], [50], [51], [74], [112], [143], [162], [163], and camera motion estimation [9], [28], [42]–[44], [44]–[46], [48], [52]–[54], [70], [84], [85], [92], [93], [99]–[102], [107] to name a few. The goal of multiview super-resolution is to reconstruct a high resolution (HR) image by fusing a sequence of degraded or aliased low resolution (LR) images of the same scene, where degradation can be a consequence of motion, camera optics, atmospheric distortions, undersampling, etc.

Multispectral sensors typically provide low-spatial high-spectral resolution for the multispectral (MS) volume, and high-spatial low-spectral resolution for the panchromatic (PAN) images. This is often due to technological limitations inherent in satellite sensors. However, numerous remote sensing applications related to land-cover management, environmental monitoring, weather forecasting, and topographic map updating require high-spatial high-spectral resolution MS image volume.

In order to obtain high spatial resolution MS images, a large body of research is devoted to fusing information of MS and PAN bands, which is called pansharpening. These methods do not consider the temporal information captured by the sensors. Multiframe SRR methods, on the other hand, fuse a sequence of degraded or aliased low resolution (LR) images of the same scene taken at different times, from different viewpoints or by different sensors, to obtain a high resolution (HR) image. Fig. I shows an example of multispectral images taken at different times by the same sensor (i.e. Landsat 7 ETM+). Approaches to solve the SRR problem can be classified into frequency domain, interpolation, regularization, and learning-based methods [158].

Fourier-based methods [118], [159], [160] use the aliasing property of LR images in order to reconstruct an HR image. Although these methods are intuitive and have low computational complexity, due to their global nature, they only allow linear space invariant blur (PSF); and it is difficult to identify a global frequency-domain *a priori* knowledge to overcome ill-posedness. Some examples of Fourier domain techniques include the works by; Tsai and Huang [159] which exploits the relationship between Continuous Fourier Transform (CFT) of the unknown HR scene and Discrete Fourier Transform (DFT) of the shifted and sampled LR images, Robinson et al. [118] which applies combined Fourier-wavelet de-convolution and de-noising algorithm, and Vandewalle et al. [160] where joint registration and reconstruction is performed using multiple unregistered images. Spatial-domain interpolation-based methods [77], [168] tackle Fourier-domain obstacles by fusing the information from all LR images using a general interpolation technique (e.g. nearest neighbor, bilinear, bicubic). However, these methods result in overly smoothed images. As examples of interpolation based methods, Irani and Peleg [77] update the HR estimate by iteratively back-projecting the difference between the approximation and exact image, and Zhou et al.



Fig. 1. Landsat 7 ETM+ multispectral images taken at different dates (shown in green areas) around Sea of Marmara.

[168] utilize multi-surface fitting. In order to stabilize the ill-posed problem of SRR, regularization-based methods [62], [108] optimize a cost function with a regularization term by incorporating prior knowledge, where probabilistic estimators such as the maximum likelihood [60], maximum *a posteriori* (MAP) [136], and Bayesian [21], [36] can be employed. The drawbacks and challenges in these methods are determination of the prior model, high computational cost, and over-smoothing. More examples of regularization-based methods include the works by Marquina and Osher [108] that employs Bregman iteration for Total Variation Regularization, and Farsiu et al. [62] in which a multi-term cost function is minimized. Finally, learning based methods [73], [76], [161], [166] obtain an HR image from a single image by utilizing training sets of LR/HR images or patch pairs. The problems with these methods include their high computational cost, and correspondence ambiguities between HR and LR images. Clustering and supervised neighbor embedding is employed by Zhang et al. [166]. Moreover, Glasner et al. [76] combine multi-image super resolution and example-based approaches based on the assumption that patches in natural images recur many times inside the image. In order to overcome the drawbacks of aforementioned methods, recent research in SRR explores wavelet-based techniques [57], [58], [79], [118]). The intuition behind these approaches is that the LR images can be used to model the lowpass subband of the unknown HR image, in order to reconstruct the high frequency information lost during image acquisition.

Li et al. [104] propose a wavelet-based multiframe SRR technique, where temporal information of low-spatial-resolution MS images are used to increase their spatial resolution, as opposed to the pansharpening methods, where PAN images are employed instead of temporal data. They propose using an SRR method based on MAP with a universal Hidden Markov Tree model as a preprocessing step for multispectral image classification, where SRR is applied band-by-band to multispectral images captured on different dates. However, although their method uses the temporal information, it does not take advantage of the high spatial resolution PAN image available with most multispectral sensors.

In this paper, we propose a wavelet-based multiframe SRR method that takes advantage of both temporal and spatial information captured by multispectral sensors, in order to obtain a higher spatial resolution MS image, which exceeds the spatial resolution of the available PAN image, while preserving the high spectral resolution. To this end, we first apply pansharpening to a set of multispectral and corresponding PAN images taken at different times, in order to obtain high spatial resolution MS images. We then use our proposed wavelet-based approach for SRR band-by-band on the pansharpened MS images, in order to achieve a higher spatial resolution MS image. In addition to simultaneous pansharpening and SRR our work makes the following contributions: (i) We assume that pansharpened MS images (i.e. LR) correspond to the approximation coefficients of the first level discrete wavelet transform (DWT) of an unknown higher spatial resolution MS image (i.e. HR) and use their second level detail coefficients for initialization (initial estimate of the high frequency content of the HR image); (ii) We establish explicit closed-form expressions that define how the local high-frequency information that we aim to recover

for the HR image are related to the local low frequency information in the given sequence of LR views (i.e. wavelet domain in-band relations across LR images). The derived formulae are provided utilizing the Haar DWT due to their simplicity and low computational requirements. However, a general formulation for other types of wavelets can be readily derived in a similar manner. (iii) We solve the newly formulated SRR problem in an iterated back-projection optimization framework that focuses solely on recovering the high-frequency information across multiple pansharpened images, i.e. recovering only the wavelet detail coefficients of the HR image (unlike typical multi-frame methods that try to recover the HR image at all frequencies by fusion of LR images). In that sense, our method is similar to single-image SRR, while still extracting information across multiple images. Our superior results can be attributed to the exactness (closed-form), well-posedness, and the linearity of the equations derived in Section IV, and the inherent nature of wavelets, making them very effective in simultaneous signal information localization in space-time-frequency.

The remainder of this paper is organized as follows. In Section II, a brief summary of related research is provided. The pansharpening method employed in this paper is explained in Section III. Sections IV and V present the derived closed-form linear relationships for wavelet coefficients, and the proposed approach for SRR, respectively. In Section VI, we present the experimental results and the comparisons. Finally, we conclude our paper in Section VII with some closing remarks.

II. RELATED WORK

Wavelet-based SRR approaches can be summarized as follows. In order to reduce noise in SRR methods, Robinson et al. [118] apply a combined Fourier-wavelet deconvolution and denoising algorithm to multiframe SRR. On the other hand, to reduce degradation artifacts such as blurring and the ringing effect, Temizel and Vlachos [157] utilize zero padding in the wavelet domain followed by cycle spinning. Zhao et al. [167] solve a constrained optimization problem utilizing wavelet domain Hidden Markov Tree (HMT) model to solve the prior knowledge problem, since HMT characterizes the statistics of real world images accurately. Nguyen and Milanfar [114], unlike the conventional interpolation based methods, use the regularity and structure in the interlaced sampling of LR images. For deblurring, Chan et al. [55] derive iterative algorithms, which decompose the HR image obtained from an iteration into different frequency components and add them to the next iteration. Ji and Fermuller [79] handle image registration and reconstruction together, by first estimating the homographies between multiple images, then reconstruct the HR image in a wavelet-based iterative back-projection scheme. Jiji et al. [80], as an example to learning-based methods, handle the problem of representing the relationship between LR-HR frames with training their dataset with HR images by learning from wavelet coefficients at finer scales, followed by regularization in a least-squares manner. The work in [75] follows Jiji's method and employs discrete wavelet transform for training, where a cost function based on MAP estimation is optimized with gradient descent method, employing an Inhomogeneous Gaussian Markov random field prior. Dong et al. [58] learn various sets of bases from a precollected dataset of example image patches, and select one set of bases adaptively to characterize the local sparse wavelet domain. The above stated methods are performed either iteratively which requires high computational time or based on interpolation which results in overly smooth images. Our goal is to derive a direct relationship between LR images for a closed-form SRR solution, which prevents sacrificing high quality.

SRR methods are widely utilized for remote sensing. Demirel and Anbarjafari [57] use DWT and an intermediate stage for estimating high frequency information for satellite image super-resolution. Patel and Joshi [116] propose a learning-based approach for SRR of hyperspectral images using the DWT, where application-specific wavelet basis (i.e. filter coefficients) are designed. Moreover, Zhang et al. [165] propose a MAP-based multiframe SRR method for hyperspectral images, where PCA is employed in order to reduce the computational complexity.

III. PANSHARPENING TECHNIQUE

Based on the main technique used, pansharpening methods can be categorized into five groups [8] as component substitution, relative spectral contribution, high-frequency injection, image statistics based, and multiresolution. Component substitution methods upsample and transform MS images and substitute components of the transformed MS bands with components from the PAN images (e.g. Intensity-Hue-Saturation (IHS) pansharpening, principal component substitution, and Gram-Schmidt spectral sharpening). Relative spectral contribution approach, on the other hand, employ a linear combination of bands instead of using substitution (e.g. Brovey transform). High-frequency injection techniques transfer the high frequency content of the PAN image to the MS images (e.g. the High Pass Modulation method); whereas image statistics based models use the statistical relationship between each band of the MS and PAN images (e.g. Bayesian based techniques and Price's method). Finally, multiresolution methods decompose MS and PAN images into different spatial levels to demonstrate the relationship between PAN and MS images in coarser scales and improve spatial details (e.g. Laplacian pyramid, wavelet, and contourlet based methods).

Wavelet-based pansharpening methods include the works by Zhou et al. [169] which merge images by performing an inverse DWT using the approximation image from each Landsat TM band and detail images from SPOT PAN, the work by Kim et al. [103], where an improved additive-wavelet fusion method is proposed using the à trous algorithm which does not decompose the MS image and inject high frequency following the frequency of the MS image using a low-resolution PAN image; and

the work by Ranchin et al. [117] where two multiscale models and two inter-band structure models are described for ARSIS concept. Alparone et al. [7] compare several methods and conclude that the multiresolution based ones and the methods that employ adaptive models for the injection of highpass details outperform all the others.

Based on the comparison results obtained by Alparone et al. [7] and Bovolo et al. [37], and the nature of the proposed method in terms of wavelet domain relations described in the next section, the Additive Wavelet Luminance Proportional (AWLP) method [115] is chosen for our framework. The AWLP method is an extended version of the additive wavelet luminance technique (AWL), which is designed for three-band (RGB) multispectral images and works in the IHS domain. The AWL method injects high frequency information of the PAN image to MS images proportional to their original values in order to preserve the radiometric signature of MS images. The AWLP method generalizes the AWL method to include arbitrary number of bands, as follows:

$$HR_i = LR_i + \frac{LR_i}{\sum_{i=1}^L LR_i} \sum_{j=1}^n w_{PAN} \quad (1)$$

where LR and HR are low and high spatial resolution MS images, respectively, L is the number of bands, n is the number of DWT decomposition levels, and w_{PAN} is the DWT decomposition of the PAN image.

IV. INTER-SUBBAND RELATIONSHIPS

In this section, the relationships between wavelet subbands of multitemporal images are derived in terms of in-band (wavelet domain) shifts of the reference image subbands. We first summarize the notation used throughout the paper.

A. Notation

Here, we provide the notation used, in Table I.

TABLE I
NOTATION

I	Reference HR image
$\mathbf{A}, \mathbf{a}, \mathbf{b}, \mathbf{c}$	Haar wavelet transform approximation, horizontal, vertical, and diagonal subbands of HR image, respectively
$\mathbf{F}, \mathbf{K}, \mathbf{L}$	Coefficient matrices to be multiplied by approximation, horizontal, vertical, and diagonal DWT subbands
h	Number of hypothetically added levels in case of non-integer shifts
s	Integer shift amount after the hypothetically added levels (h)

Bold letters in the following sections demonstrate matrices and vectors. Subscripts x and y indicate the horizontal and vertical translation directions, respectively.

B. In-band Shifts

As a wavelet-based SRR method, our goal is to reconstruct an HR image (i.e. HR MS) using the given LR sequence (i.e. pansharpened MS images) assumed to represent the lowpass subbands of an unknown HR sequence of images. Therefore, we derive the relationships between the DWT subbands of the reference images and the target HR images, assuming that their lowpass subbands are the given LR images for SRR. To derive the closed-form relationships, we assume that HR images are given, and describe in-band shifts (in the wavelet domain) of the reference HR image subbands. For the SRR method, we inverse the process and use these relationships as our model, in order to estimate the high-frequency information of the unknown reference HR image, given lowpass subbands. Below, we derive the mathematical expressions which demonstrate these relationships.

Let A , a , b , and c be the first level approximation, horizontal, vertical, and diagonal detail coefficients (subbands), respectively, of a 2D reference HR image, I , of size $2m \times 2n$, where m and n are positive integers. Since decimation operator in DWT reduces the size of input image by half in each direction for each subband, we require the image sizes to be divisible by 2. Now, the 1st level Haar transform subbands of the target HR image translated in any direction (i.e. horizontal, vertical, diagonal), can be expressed in matrix form using the 1st level subbands of the reference HR image as in the following equations (also illustrated in Fig. 2):

$$\begin{aligned} \mathbf{A}_s &= \mathbf{F}_y \mathbf{A} \mathbf{F}_x + \mathbf{F}_y \mathbf{a} \mathbf{K}_1 + \mathbf{L}_1 \mathbf{b} \mathbf{F}_x + \mathbf{L}_1 \mathbf{c} \mathbf{K}_1 \\ \mathbf{a}_s &= -\mathbf{F}_y \mathbf{A} \mathbf{K}_1 + \mathbf{F}_y \mathbf{a} \mathbf{K}_2 - \mathbf{L}_1 \mathbf{b} \mathbf{K}_1 + \mathbf{L}_1 \mathbf{c} \mathbf{K}_2 \\ \mathbf{b}_s &= -\mathbf{L}_1 \mathbf{A} \mathbf{F}_x - \mathbf{L}_1 \mathbf{a} \mathbf{K}_1 + \mathbf{L}_2 \mathbf{b} \mathbf{F}_x + \mathbf{L}_2 \mathbf{c} \mathbf{K}_1 \\ \mathbf{c}_s &= \mathbf{L}_1 \mathbf{A} \mathbf{K}_1 - \mathbf{L}_1 \mathbf{a} \mathbf{K}_2 - \mathbf{L}_2 \mathbf{b} \mathbf{K}_1 + \mathbf{L}_2 \mathbf{c} \mathbf{K}_2 \end{aligned} \quad (2)$$

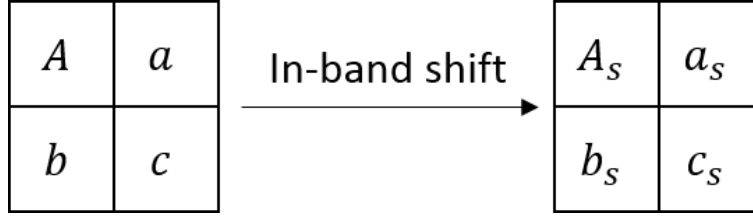


Fig. 2. In-band shift of reference image subbands.

As already mentioned in Section IV-A, \mathbf{F} , \mathbf{K} , and \mathbf{L} stand for coefficient matrices to be multiplied by the lowpass and highpass subbands of the reference HR image, where subscripts x and y indicate *horizontal* and *vertical* shifts. $\mathbf{A}_s, \mathbf{a}_s, \mathbf{b}_s, \mathbf{c}_s$ are translated (i.e. target) HR image subbands in any direction. The low/highpass subbands of both reference and target images are of size $m \times n$, \mathbf{F}_y and $\mathbf{L}_{1,2}$ are $m \times m$, whereas \mathbf{F}_x and $\mathbf{K}_{1,2}$ are $n \times n$.

By examining the translational shifts between subbands of two input frames in the Haar domain, we realize that horizontal translation reduces \mathbf{L} to zero and \mathbf{F}_y to the identity matrix. This could be understood by examining the coefficient matrices defined later in this section (namely, Eq. (4)), by setting the related vertical components to zero (specifically, s_y and h_y). Likewise, vertical translation depends solely on approximation and vertical detail coefficients, in which case \mathbf{K} is reduced to zero and \mathbf{F}_x is equal to the identity matrix.

Here, we first define the matrices for subpixel shift amounts. The algorithm to reach any shift amount using the subpixel relationship will be described later in this section.

Contrary to the customary model of approximating a subpixel shift by upsampling an image followed by an integer shift, our method models subpixel shift directly based on the original coefficients of the reference HR image, without upsampling and the need for interpolation. To this end, we resort to the following observations:

(1) Upsampling an image I , is equivalent to adding levels to the bottom of its wavelet transform, and setting the detail coefficients to zero, while the approximation coefficients remain the same, as demonstrated in Fig. 3 for upsampling by 2^1 as an example, where gray subbands show added zeros.

(2) Shifting the upsampled image by an amount of s is equivalent to shifting the original image by an amount of $s/2^h$, where h is the number of added levels (e.g. $h = 1$ in Fig. 3).

These observations allow us to perform in-band shift of the reference image subbands for a subpixel amount, without upsampling or interpolation. Transformed images, therefore, can be found by using the original level subbands of the reference HR image with the help of a hypothetically added level (h) and an integer shift value (s) at the added level.

Now, the aforementioned coefficient matrices, \mathbf{F}_x , \mathbf{K}_1 , and \mathbf{K}_2 can be defined, in lower bidiagonal Toeplitz matrix form as follows.

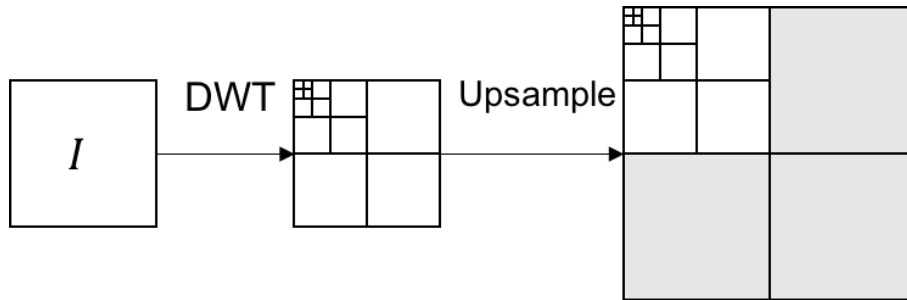


Fig. 3. Illustration of upsampling process.

$$\mathbf{F}_x = \frac{1}{2^{h_x+1}} \begin{bmatrix} 2^{h_x+1} - |s_x| & & & & \\ |s_x| & 2^{h_x+1} - |s_x| & & & \\ & |s_x| & \ddots & \ddots & \\ & & & |s_x| & 2^{h_x+1} - |s_x| \end{bmatrix}$$

$$\mathbf{F}_y = \frac{1}{2^{h_y+1}} \begin{bmatrix} 2^{h_y+1} - |s_y| & |s_y| & & & \\ & 2^{h_y+1} - |s_y| & |s_y| & & \\ & & \ddots & \ddots & \\ & & & \ddots & |s_y| \end{bmatrix} \quad (3)$$

$$\mathbf{K}_1 = \frac{1}{2^{h_x+1}} \begin{bmatrix} -s_x & & & & \\ s_x & -s_x & & & \\ & s_x & & & \\ & & \ddots & \ddots & \\ & & & s_x & -s_x \end{bmatrix}$$

$$\mathbf{L}_1 = \frac{1}{2^{h_y+1}} \begin{bmatrix} -s_y & s_y & & & \\ & -s_y & s_y & & \\ & & \ddots & \ddots & \\ & & & -s_y & s_y \\ & & & & -s_y \end{bmatrix}$$

$$\mathbf{K}_2 = \frac{1}{2^{h_x+1}} \begin{bmatrix} 2^{h_x+1} - 3|s_x| & & & & \\ -|s_x| & 2^{h_x+1} - 3|s_x| & & & \\ & -|s_x| & & & \\ & & \ddots & \ddots & \\ & & & -|s_x| & 2^{h_x+1} - 3|s_x| \end{bmatrix} \quad (4)$$

$$\mathbf{L}_2 = \frac{1}{2^{h_y+1}} \begin{bmatrix} 2^{h_y+1} - 3|s_y| & -|s_y| & & & \\ & 2^{h_y+1} - 3|s_y| & -|s_y| & & \\ & & \ddots & \ddots & \\ & & & -|s_y| & 2^{h_y+1} - 3|s_y| \end{bmatrix} \quad (5)$$

where s_x and h_x demonstrate the integer shift amount at the hypothetically added level and the number of added levels for x direction, respectively.

\mathbf{F}_y , \mathbf{L}_1 , and \mathbf{L}_2 matrices are defined in a similar manner by upper bidiagonal Toeplitz matrices, using y direction values for s and h . When the shift amount is negative, diagonals of the coefficient matrices interchange.

As mentioned earlier, \mathbf{F}_x and $\mathbf{K}_{1,2}$ are $n \times n$, while \mathbf{F}_y and $\mathbf{L}_{1,2}$ are $m \times m$. Sizes of these matrices also indicate that in-band shift of subbands is performed using only the original level Haar coefficients (which are of size $m \times n$) without upsampling.

The relationship defined above for subpixel shifts, can be used to produce any shift amount based on the fact that wavelet subbands are periodically shift-invariant. Table II demonstrates the calculation of any shift using subpixels, where % stands for modulo, $\lfloor s \rfloor$ and $\lceil s \rceil$ are the greatest integer lower than, and smallest integer higher than the shift, s . Performing circular shift of subbands for given values in each shift amount case, and setting the new shift amount to the new shifts in Table II, we can calculate any fractional or integer amount of shifts using subpixels.

TABLE II
ARBITRARY SHIFTS BASED ON CIRCULAR SHIFT AND SUBPIXEL VALUES

Shift amount	Circular shift	New shift amount
$s \% 2 = 0$	$s/2$	0
$s \% 2 = 1$	$\lfloor s/2 \rfloor$	1
$\lceil s \rceil \% 2 = 0$	$\lceil s \rceil / 2$	$s - \lceil s \rceil$
$\lfloor s \rfloor \% 2 = 0$	$\lfloor s \rfloor / 2$	$s - \lfloor s \rfloor$

If the shift amount (or the new shift in Table II) is not divisible by 2, in order to reach an integer value at the $(N + h)$ th level, the shift value at the original level is rounded to the closest decimal point which is divisible by 2^h .

V. SUPER RESOLUTION RECONSTRUCTION

In this section, we first present the SRR observation model, followed by our proposed method.

A. Observation Model

Let $I(\sigma m \times \sigma n)$ denote the desired HR image, and A_k be the k th observed LR image, with a downsampling ration of σ . The SRR observation model is given by:

$$\mathbf{A}_k = \mathbf{D}_k \mathbf{B}_k \mathbf{M}_k \mathbf{I} + \mathbf{n}_k, \quad k = 1, 2, \dots, K \quad (6)$$

where \mathbf{M}_k , \mathbf{B}_k , \mathbf{D}_k , and \mathbf{n}_k denote motion, blurring effect, downsampling operator, and noise term for the k th LR image, respectively. In the above formula, LR and HR images are rearranged in lexicographic order; therefore, \mathbf{I} is of size $\sigma^2 mn \times 1$, \mathbf{A}_k and \mathbf{n}_k are $mn \times 1$, \mathbf{B}_k and \mathbf{M}_k are $\sigma^2 mn \times \sigma^2 mn$, and \mathbf{D}_k is $mn \times \sigma^2 mn$.

Assuming the same downsampling ratio for all LR images, and taking bands of MS images into account, we can modify the above observation model as follows:

$$\mathbf{A}_{k,i} = \mathbf{D} \mathbf{B}_{k,i} \mathbf{M}_{k,i} \mathbf{I} + \mathbf{n}_{k,i} \quad (7)$$

where $k = 1, 2, \dots, K$, $i = 1, 2, \dots, L$, K is the number of LR images, and L is the number of MS bands.

Given a sequence of pansharpened MS bands, $\mathbf{A}_{k,i}$, our goal is to reconstruct the unknown HR MS image, \mathbf{I} , which exceeds the spatial resolution of the available PAN image.

B. Proposed Method

Spatial resolution of PAN images differ based on the multispectral sensors. For example, while Landsat 7 ETM+ sensors provide 15 m spatial resolution PAN images, Quickbird sensors increase this amount upto 61 cm. In order to increase the available spatial resolution of PAN images while keeping the spectral resolution provided by MS bands, we propose using both temporal and spectral information accessible via most multispectral sensors. Therefore, we first apply pansharpening to multispectral images captured around the same region at different dates. Then, using these pansharpened MS images, we perform multiframe SRR in order to exceed the spatial resolution of handy PAN images. Fig. 4 shows a pictorial explanation of the flowchart of proposed scheme.

As in the underlying idea of wavelet-based SRR algorithms, we assume that the given LR image sequence (i.e. pansharpened MS images) is the lowpass subbands of unknown HR images. The goal is to reconstruct the unknown highpass subbands of one of these HR images, chosen as the reference. The SRR method described below is the inverse process of the method described in Section IV, where HR images are unknown, and high frequency information for one of these underlying HR images is estimated by a modified iterated back projection method. We perform the proposed scheme on each band of multitemporal pansharpened MS images. Fig. 5 shows the SRR step for one band of MS images, where gray areas in dashed lines indicate unknown images and coefficients, and input LR sequence in white solid lines stand for one band of the pansharpened MS images taken at different times.

SRR process consists of two steps of image registration [6], [19], [20], [22], [24]–[27], [30], [31], [64]–[69], [71], [72], [122], [130], [131] and image reconstruction [33]–[35], [49], [78], [105], [119]–[121], [123]–[129], [132], [133], [135]. For the image registration step, we employed a method which uses SURF [32] and RANSAC [63], implemented in IAT toolbox [61], where reference and target images are registered for affine transform. Since we assume that bands of an MS image captured by the same sensor are already aligned, we perform registration on one band only, and apply the same registration parameters to all bands. Once registration parameters are estimated, target images are rotated back for the estimated rotation amount in order for LR images to have only translational transform between them, since the formulae in Section IV are derived for translational shifts.

As a modification to the general Iterated Back Projection algorithm described first by Irani and Peleg [77], we use the proposed method in Section IV to simulate motion. As in [118], we change the order of motion and blur matrices in the SRR observation model as in:

$$\mathbf{A}_{k,i} = \mathbf{D} \mathbf{M}_{k,i} \mathbf{B}_{k,i} \mathbf{I} + \mathbf{n}_{k,i} \quad (8)$$

Since our model uses wavelet decomposition of a reference image, in order to estimate the target images, the proposed method fuses the matrices \mathbf{D} and $\mathbf{M}_{k,i}$:

$$\mathbf{A}_{k,i} = \mathbf{m}_{k,i} \mathbf{B}_{k,i} \mathbf{I} + \mathbf{n}_{k,i} \quad (9)$$

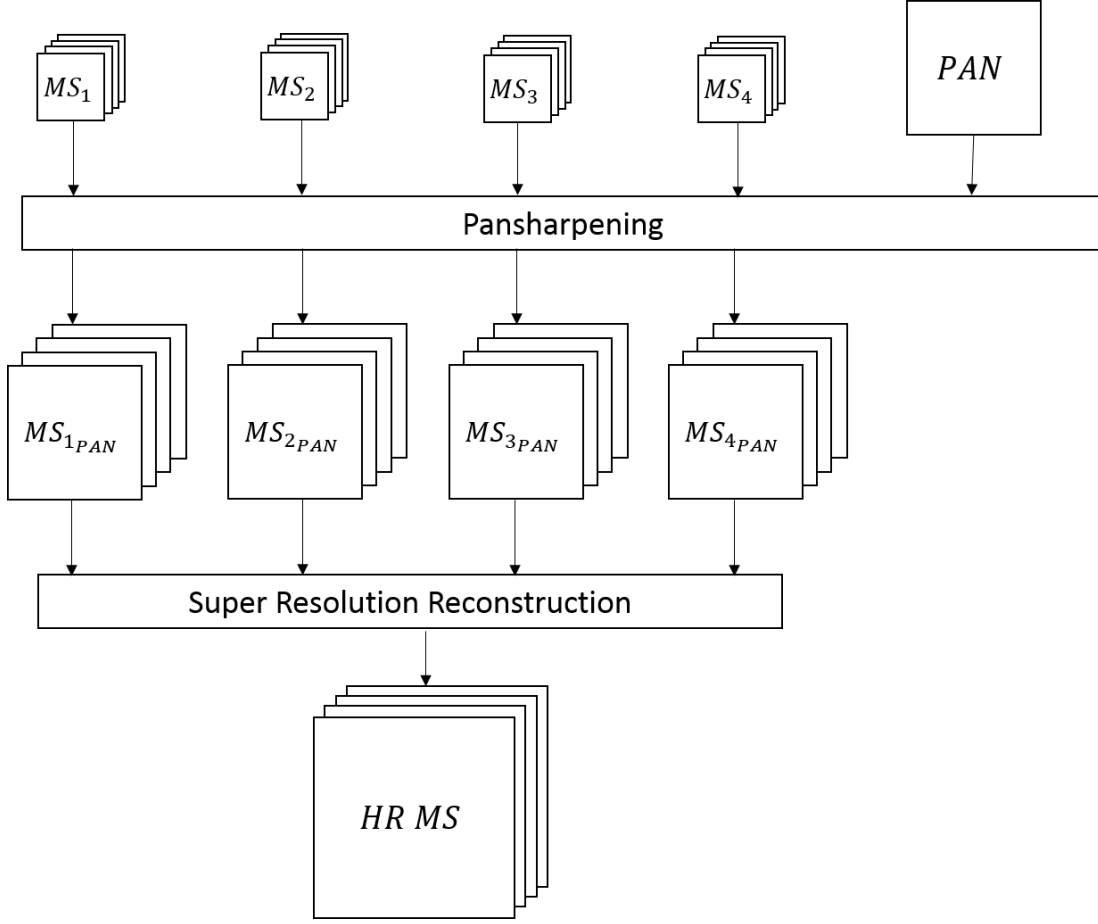


Fig. 4. Flowchart of the proposed method.

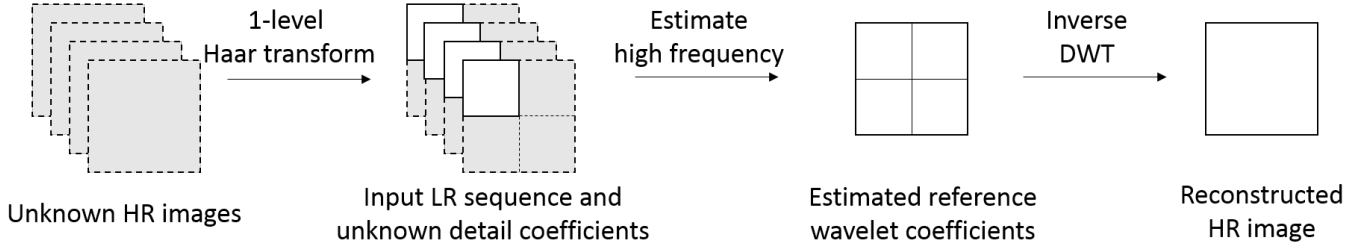


Fig. 5. SRR for one band of MS image.

where $\mathbf{m}_{k,i} = \mathbf{D} * \mathbf{M}_{k,i}$ with $k = 1, 2, \dots, K$, $i = 1, 2, \dots, L$, as defined before.

High resolution image is then estimated by the following formula which is shown for one band:

$$\hat{\mathbf{I}}^{(n+1)} = \hat{\mathbf{I}}^{(n)} + \lambda \sum_k (\mathbf{A}_k - \hat{\mathbf{A}}_k) h^{BP} \quad (10)$$

where n stands for the iteration number, λ is a step size, $\hat{\mathbf{A}}_k$ is estimated using current I and motion parameters, and h^{BP} is a back projection kernel as defined in [77].

The relationship between two translated LR images (i.e. \mathbf{A} and \mathbf{A}_s in Section IV) depends on the highpass subband of the reference HR image (i.e. \mathbf{a} , \mathbf{b} , \mathbf{c}). This fact is used to construct a linear system of equations based on known LR images and unknown highpass subbands of the reference HR image using related formulae from Eq. (2) for each target LR image. Since there are three unknowns (horizontal, vertical, and diagonal detail coefficients of the unknown HR image), at least three shifted LR images together with the reference LR image are required to solve the linear system. In order to avoid instabilities caused by inversion, the system is solved in an iterative least squares fashion. The linear system can be constructed as follows:

$$\begin{aligned}
\mathbf{A}_{s_1} &= \mathbf{F}_{y_1} \mathbf{A} \mathbf{F}_{x_1} + \mathbf{F}_{y_1} \mathbf{a} \mathbf{K}_{1_1} + \mathbf{L}_{1_1} \mathbf{b} \mathbf{F}_{x_1} + \mathbf{L}_{1_1} \mathbf{c} \mathbf{K}_{1_1} \\
\mathbf{A}_{s_2} &= \mathbf{F}_{y_2} \mathbf{A} \mathbf{F}_{x_2} + \mathbf{F}_{y_2} \mathbf{a} \mathbf{K}_{1_2} + \mathbf{L}_{1_2} \mathbf{b} \mathbf{F}_{x_2} + \mathbf{L}_{1_2} \mathbf{c} \mathbf{K}_{1_2} \\
\mathbf{A}_{s_3} &= \mathbf{F}_{y_3} \mathbf{A} \mathbf{F}_{x_3} + \mathbf{F}_{y_3} \mathbf{a} \mathbf{K}_{1_3} + \mathbf{L}_{1_3} \mathbf{b} \mathbf{F}_{x_3} + \mathbf{L}_{1_3} \mathbf{c} \mathbf{K}_{1_3}
\end{aligned} \tag{11}$$

By rearranging (11), we find:

$$\mathbf{A}_{s_i} = (\mathbf{F}_{y_i} \otimes \mathbf{F}'_{x_i}) \mathbf{A} + (\mathbf{F}_{y_i} \otimes \mathbf{K}'_{1_i}) \mathbf{a} + (\mathbf{L}_{1_i} \otimes \mathbf{F}'_{x_i}) \mathbf{b} + (\mathbf{L}_{1_i} \otimes \mathbf{K}'_{1_i}) \mathbf{c} \tag{12}$$

where $i = 1, 2, 3$. Here, \mathbf{A}_{s_i} , \mathbf{A} , \mathbf{a} , \mathbf{b} , and \mathbf{c} are rearranged as $mn \times 1$ vectors, Kronecker tensor products in parenthesis are $mn \times mn$.

In order to solve the system in Eq. (12) in a least squares manner, by reorganizing, we have;

$$\begin{bmatrix} \mathbf{A}_{s_1} \\ \mathbf{A}_{s_2} \\ \mathbf{A}_{s_3} \end{bmatrix} = \begin{bmatrix} \mathbf{F}_{y_1} \otimes \mathbf{F}'_{x_1} \\ \mathbf{F}_{y_2} \otimes \mathbf{F}'_{x_2} \\ \mathbf{F}_{y_3} \otimes \mathbf{F}'_{x_3} \end{bmatrix} \mathbf{A} + \begin{bmatrix} \mathbf{F}_{y_1} \otimes \mathbf{K}'_{1_1} & \mathbf{L}_{1_1} \otimes \mathbf{F}'_{x_1} & \mathbf{L}_{1_1} \otimes \mathbf{K}'_{1_1} \\ \mathbf{F}_{y_2} \otimes \mathbf{K}'_{1_2} & \mathbf{L}_{1_2} \otimes \mathbf{F}'_{x_2} & \mathbf{L}_{1_2} \otimes \mathbf{K}'_{1_2} \\ \mathbf{F}_{y_3} \otimes \mathbf{K}'_{1_3} & \mathbf{L}_{1_3} \otimes \mathbf{F}'_{x_3} & \mathbf{L}_{1_3} \otimes \mathbf{K}'_{1_3} \end{bmatrix} \begin{bmatrix} \mathbf{a} \\ \mathbf{b} \\ \mathbf{c} \end{bmatrix} \tag{13}$$

Finally, the system in Eq. (13) is solved by minimizing the following cost function:

$$\begin{bmatrix} \hat{\mathbf{a}} \\ \hat{\mathbf{b}} \\ \hat{\mathbf{c}} \end{bmatrix} = \arg \min \left\| \begin{bmatrix} \mathbf{F}_{y_1} \otimes \mathbf{K}'_{1_1} & \mathbf{L}_{1_1} \otimes \mathbf{F}'_{x_1} & \mathbf{L}_{1_1} \otimes \mathbf{K}'_{1_1} \\ \mathbf{F}_{y_2} \otimes \mathbf{K}'_{1_2} & \mathbf{L}_{1_2} \otimes \mathbf{F}'_{x_2} & \mathbf{L}_{1_2} \otimes \mathbf{K}'_{1_2} \\ \mathbf{F}_{y_3} \otimes \mathbf{K}'_{1_3} & \mathbf{L}_{1_3} \otimes \mathbf{F}'_{x_3} & \mathbf{L}_{1_3} \otimes \mathbf{K}'_{1_3} \end{bmatrix} \begin{bmatrix} \mathbf{a} \\ \mathbf{b} \\ \mathbf{c} \end{bmatrix} - \left(\begin{bmatrix} \mathbf{A}_{s_1} \\ \mathbf{A}_{s_2} \\ \mathbf{A}_{s_3} \end{bmatrix} - \begin{bmatrix} \mathbf{F}_{y_1} \otimes \mathbf{F}'_{x_1} \\ \mathbf{F}_{y_2} \otimes \mathbf{F}'_{x_2} \\ \mathbf{F}_{y_3} \otimes \mathbf{F}'_{x_3} \end{bmatrix} \mathbf{A} \right) \right\|^2 \tag{14}$$

where $\hat{\mathbf{a}}, \hat{\mathbf{b}}, \hat{\mathbf{c}}$ are estimated high-pass subbands of the underlying unknown reference HR image. Once this system is solved, inverse Haar transform utilizing the reference LR image and the estimated highpass subbands gives the reconstructed HR image.

The proposed algorithm can also be explained step by step as in **Algorithm** - Super Resolution Reconstruction of Pansharp-ened MS images.

Algorithm *SRR of Pansharp-ened MS images*

- *Input*: Multitemporal MS and PAN bands
- *Objective*: Reconstruct high resolution MS images, exceeding the PAN band spatial resolution
- *Output*: High spatial/spectral resolution MS images
- Pansharpening
 - ◊ Perform pansharpening using AWLP
- SRR Process — do for each pansharp-ened MS band
 - ◊ Image registration
 - * Choose a reference image
 - * Register all target images to reference
 - * Eliminate rotation for all target images
 - ◊ Image reconstruction
 - * Construct coefficient matrices defined in Section IV for all LR images, using registration parameters found for translation
 - * Initialize HR image
 - * Do
 - Perform Haar transform on HR image
 - Use wavelet subbands with constructed matrices to estimate LR images
 - Update HR using Eq. (10)
 - * while $MSE(\mathbf{A}_k - \hat{\mathbf{A}}_k) > \tau$, where τ is a predefined tolerance for error.

VI. EXPERIMENTAL RESULTS

We test our proposed method using Landsat 7 ETM+ images taken at different dates, which have seven MS bands together with a PAN band. The spectral resolution of MS bands range from $0.45\mu\text{m}$ to $2.35\mu\text{m}$, while PAN bands span $0.52 - 0.9\mu\text{m}$ spectrum; and the spatial resolution of MS bands are 30 m, whereas PAN bands are 15 m. We select four multispectral image groups together with their PAN bands from a region in Marmara Sea, captured on July 2, September 4, in 2000, and May 18, August 6, in 2001. We conduct two sets of tests which are categorized as simulated and real experiments. All tests are carried after MS and PAN bands are fused in pansharpening.

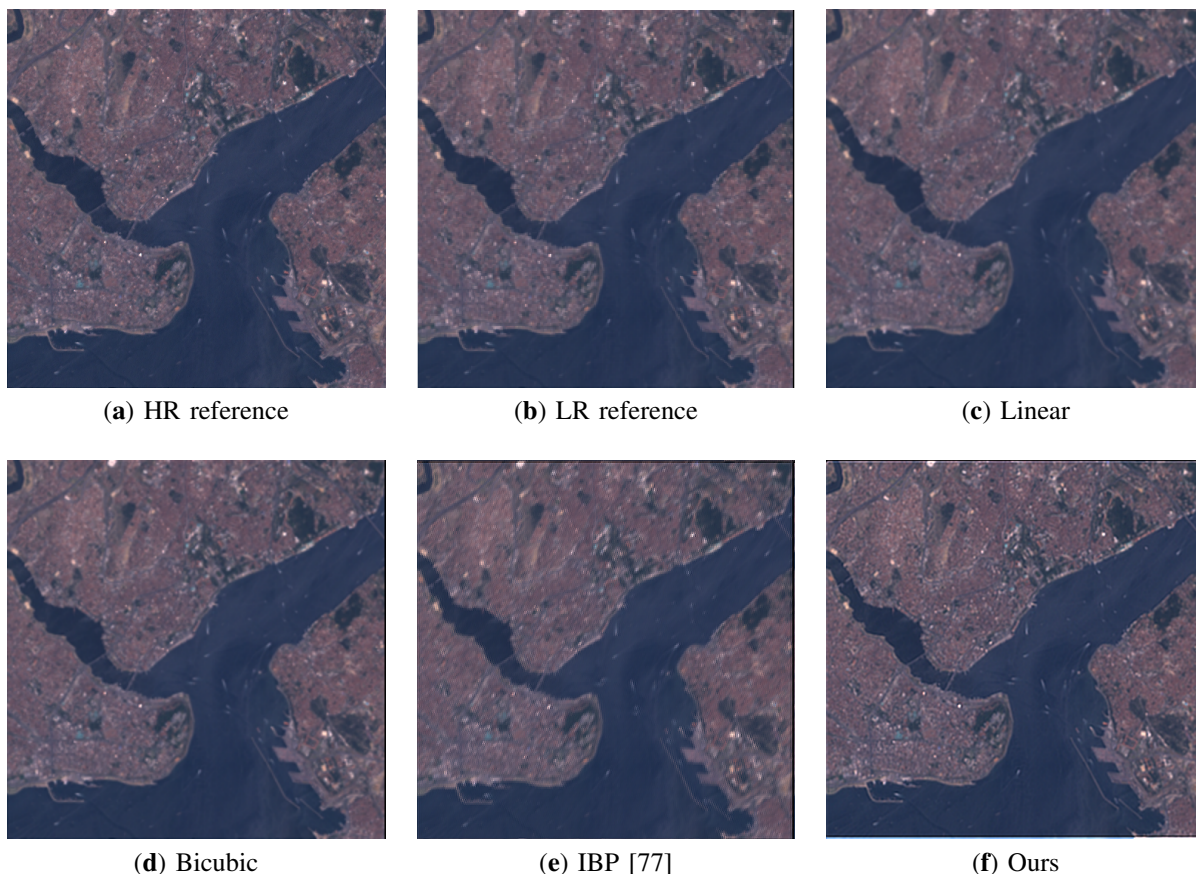


Fig. 6. Simulated results comparison of different methods with the reference image See the text and Table III for more details.

A. Simulated Dataset

Our first test is a simulated experiment, where one of the pansharpened MS images is chosen as reference, shifted in horizontal, vertical, and diagonal directions for one pixel, convolved with a Gaussian filter, and downsampled, which is a conventional method used for simulated SRR experiments [165]. The pansharpened MS image chosen as reference is then used as the ground truth in comparisons.

For image registration, one of the bands of the reference pansharpened MS image is chosen as the reference band, and image registration is performed for the same band of all datasets. Rotation is recovered for all target image bands, in order to have only translation between LR sets. Since we define our in-band shift method using subpixels and circular shifts, image regions are adjusted in order to cover the same area. We then initialize our HR estimate using the inverse transform of known reference LR and upsampled wavelet subbands of the LR image. The iterative method described in Section V is then applied in order to estimate the final HR image. We compare our results both qualitatively and quantitatively with conventional interpolation techniques and the IBP method [77], since we propose a modified IBP model. All compared methods are given the same pansharpened MS images as input. Quantitative comparisons are based on Peak-Signal-to-Noise-Ratio (PSNR), Mean Square Error (MSE) and Structural Similarity Index (SSIM).

Fig. 6 (a) shows the reference image used in simulated tests, which is from a region in Istanbul, Turkey, captured on July 2, 2000. All figures for simulated and real experiments, show a composite of R, G, and B bands.

Fig. 6 shows reference HR and reference LR images together with the compared methods including Bilinear interpolation, Bicubic interpolation and IBP method. In order to comprehend the results, 7 provides zoomed in areas of all images in 6. As can be seen from these figures, the proposed method preserves spectral information of the MS bands while increasing the spatial resolution. Figures confirm that the proposed method reconstructs edges better than the compared ones.

Table III provides the quantitative comparisons based on PSNR, MSE and SSIM values for each band, for a resolution enhancement factor of two. Since pansharpening methods use MS bands numbered 1, 2, 3, 4, 5, and 7 for Landsat 7 ETM+, we compare the results for these bands. Quantitative comparisons in the table also validate the qualitative illustrations in the figures. Even though for some bands, the results obtained with the proposed method is lower than the compared ones, in general the proposed method preserves the spectral information better while increasing the spatial resolution.

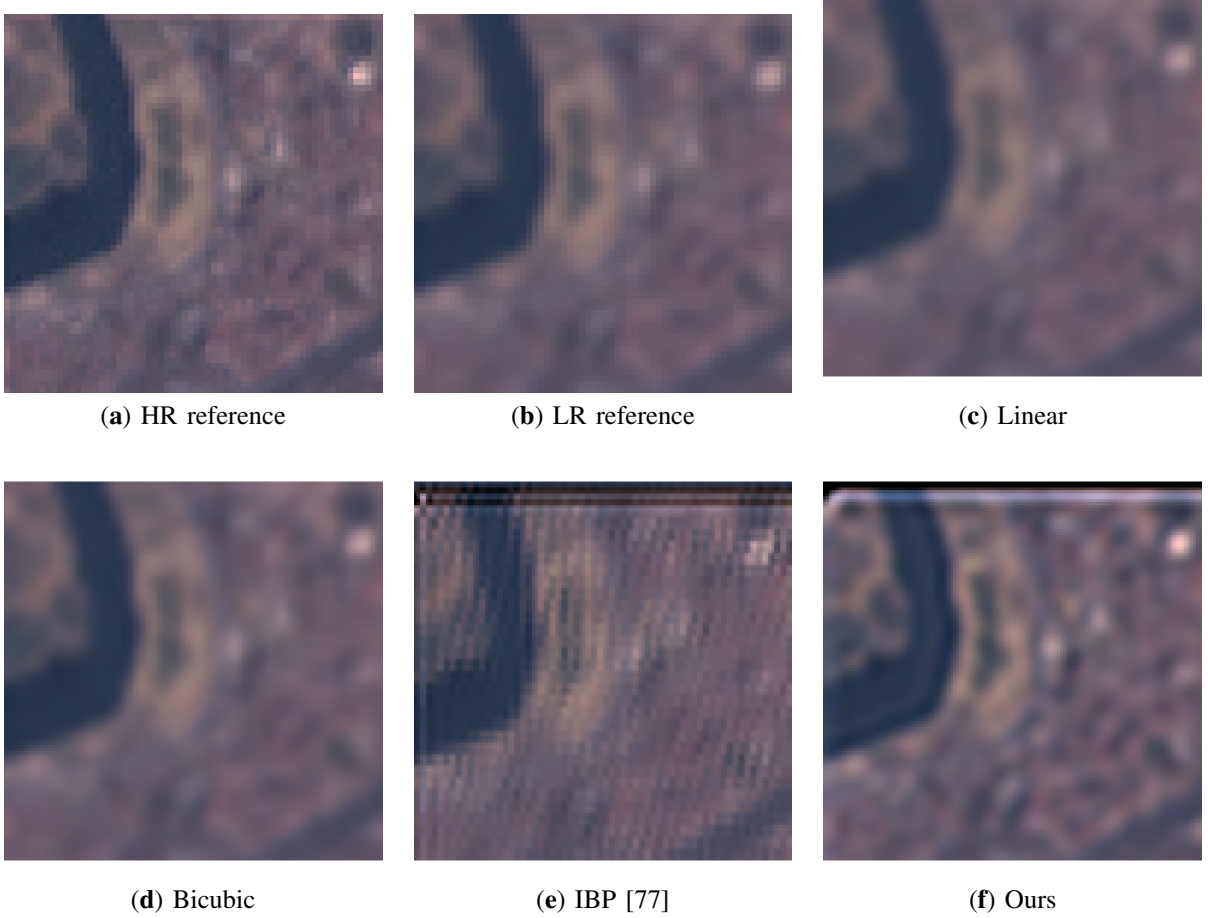


Fig. 7. Simulated results: comparison in a zoomed-in area. See the text and Table III for more details.

TABLE III
COMPARISON OF PROPOSED METHOD WITH OTHER METHODS IN PSNR, MSE, SSIM.

Band	Linear			Bicubic			IBP			Proposed		
	PSNR	MSE	SSIM	PSNR	MSE	SSIM	PSNR	MSE	SSIM	PSNR	MSE	SSIM
1	33.57	0	0.88	33.94	0	0.91	25.71	0.004	0.58	34.82	0	0.91
2	27.24	0.004	0.78	27.37	0.004	0.81	25.17	0.006	0.58	25.70	0.004	0.84
3	22.37	0.01	0.7	22.39	0.01	0.73	21.65	0.01	0.53	27.26	0.003	0.78
4	20.18	0.02	0.49	20.19	0.02	0.5	19.92	0.02	0.42	16.47	0.03	0.51
5	25.18	0.006	0.73	25.09	0.006	0.74	22.99	0.01	0.45	26.01	0.005	0.7
7	25.21	0.006	0.72	25.13	0.006	0.73	23.01	0.01	0.44	26.03	0.005	0.72

B. Real Dataset

For the second test, we use pansharpened MS bands as our LR image set, and estimate an HR image without a ground truth. This test is compared qualitatively only. Fig. VI-B shows the real dataset used for the experiments.

VII. CONCLUSION

Multispectral sensors provide low-spatial MS and high-spatial PAN images. Pansharpening or SRR methods are used separately in order to obtain high-spatial resolution MS bands without losing spectral information. In this paper, we propose employing pansharpening and SRR method together, to exceed the spatial resolution available in the PAN bands, by using both spatial and temporal information captured by most multispectral sensors. We perform pansharpening and registration before applying the proposed SRR technique, for which we derive closed-form model of wavelet domain in-band relationships. Experimental results demonstrate that the proposed scheme indeed exceeds the spatial resolution of PAN bands, while keeping the spectral information of MS bands.



Fig. 8. Real pansharpened MS images (RGB bands).

REFERENCES

- [1] Muhamad Ali and Hassan Foroosh. Natural scene character recognition without dependency on specific features. In *Proc. International Conference on Computer Vision Theory and Applications*, 2015.
- [2] Muhamad Ali and Hassan Foroosh. A holistic method to recognize characters in natural scenes. In *Proc. International Conference on Computer Vision Theory and Applications*, 2016.
- [3] Muhammad Ali and Hassan Foroosh. Character recognition in natural scene images using rank-1 tensor decomposition. In *Proc. of International Conference on Image Processing (ICIP)*, pages 2891–2895, 2016.
- [4] Mais Alnasser and Hassan Foroosh. Image-based rendering of synthetic diffuse objects in natural scenes. In *Proc. IAPR Int. Conference on Pattern Recognition*, volume 4, pages 787–790, 2006.
- [5] Mais Alnasser and Hassan Foroosh. Rendering synthetic objects in natural scenes. In *Proc. of IEEE International Conference on Image Processing (ICIP)*, pages 493–496, 2006.
- [6] Mais Alnasser and Hassan Foroosh. Phase shifting for non-separable 2d haar wavelets. *IEEE Transactions on Image Processing*, 16:1061–1068, 2008.
- [7] Luciano Alparone, Lucien Wald, Jocelyn Chanussot, Claire Thomas, Paolo Gamba, and Lori Mann Bruce. Comparison of pansharpening algorithms: Outcome of the 2006 grs-s data-fusion contest. *IEEE Transactions on Geoscience and Remote Sensing*, 45(10):3012–3021, 2007.
- [8] Israa Amro, Javier Mateos, Miguel Vega, Rafael Molina, and Aggelos K Katsaggelos. A survey of classical methods and new trends in pansharpening of multispectral images. *EURASIP Journal on Advances in Signal Processing*, 2011(1):79, 2011.
- [9] Nazim Ashraf and Hassan Foroosh. Robust auto-calibration of a ptz camera with non-overlapping fov. In *Proc. International Conference on Pattern Recognition (ICPR)*, 2008.
- [10] Nazim Ashraf and Hassan Foroosh. Human action recognition in video data using invariant characteristic vectors. In *Proc. of IEEE Int. Conf. on Image Processing (ICIP)*, pages 1385–1388, 2012.
- [11] Nazim Ashraf and Hassan Foroosh. Motion retrieval using consistency of epipolar geometry. In *Proceedings of IEEE International Conference on Image Processing (ICIP)*, pages 4219–4223, 2015.
- [12] Nazim Ashraf, Yuping Shen, Xiaochun Cao, and Hassan Foroosh. View-invariant action recognition using weighted fundamental ratios. *Journal of Computer Vision and Image Understanding (CVIU)*, 117:587–602, 2013.

- [13] Nazim Ashraf, Yuping Shen, Xiaochun Cao, and Hassan Foroosh. View invariant action recognition using weighted fundamental ratios. *Computer Vision and Image Understanding*, 117(6):587–602, 2013.
- [14] Nazim Ashraf, Yuping Shen, and Hassan Foroosh. View-invariant action recognition using rank constraint. In *Proc. of IAPR Int. Conf. Pattern Recognition (ICPR)*, pages 3611–3614, 2010.
- [15] Nazim Ashraf, Chuan Sun, and Hassan Foroosh. Motion retrieval using low-rank decomposition of fundamental ratios. In *Proc. IEEE International Conference on Image Processing (ICIP)*, pages 1905–1908, 2012.
- [16] Nazim Ashraf, Chuan Sun, and Hassan Foroosh. Motion retrieval using low-rank decomposition of fundamental ratios. In *Image Processing (ICIP), 2012 19th IEEE International Conference on*, pages 1905–1908, 2012.
- [17] Nazim Ashraf, Chuan Sun, and Hassan Foroosh. View-invariant action recognition using projective depth. *Journal of Computer Vision and Image Understanding (CVIU)*, 123:41–52, 2014.
- [18] Nazim Ashraf, Chuan Sun, and Hassan Foroosh. View invariant action recognition using projective depth. *Computer Vision and Image Understanding*, 123:41–52, 2014.
- [19] Vildan Atalay and Hassan Foroosh. In-band sub-pixel registration of wavelet-encoded images from sparse coefficients. *Signal, Image and Video Processing*, 2017.
- [20] Vildan A. Aydin and Hassan Foroosh. Motion compensation using critically sampled dwt subbands for low-bitrate video coding. In *Proc. IEEE International Conference on Image Processing (ICIP)*, 2017.
- [21] S Derin Babacan, Rafael Molina, and Aggelos K Katsaggelos. Variational bayesian super resolution. *Image Processing, IEEE Transactions on*, 20(4):984–999, 2011.
- [22] Murat Balci, Mais Alnasser, and Hassan Foroosh. Alignment of maxillofacial ct scans to stone-cast models using 3d symmetry for backscattering artifact reduction. In *Proceedings of Medical Image Understanding and Analysis Conference*, 2006.
- [23] Murat Balci, Mais Alnasser, and Hassan Foroosh. Image-based simulation of gaseous material. In *Proc. of IEEE International Conference on Image Processing (ICIP)*, pages 489–492, 2006.
- [24] Murat Balci, Mais Alnasser, and Hassan Foroosh. Subpixel alignment of mri data under cartesian and log-polar sampling. In *Proc. of IAPR Int. Conf. Pattern Recognition*, volume 3, pages 607–610, 2006.
- [25] Murat Balci and Hassan Foroosh. Estimating sub-pixel shifts directly from phase difference. In *Proc. of IEEE International Conference on Image Processing (ICIP)*, pages 1057–1060, 2005.
- [26] Murat Balci and Hassan Foroosh. Estimating sub-pixel shifts directly from the phase difference. In *Proc. of IEEE Int. Conf. Image Processing (ICIP)*, volume 1, pages I–1057, 2005.
- [27] Murat Balci and Hassan Foroosh. Inferring motion from the rank constraint of the phase matrix. In *Proc. IEEE Conf. on Acoustics, Speech, and Signal Processing*, volume 2, pages ii–925, 2005.
- [28] Murat Balci and Hassan Foroosh. Metrology in uncalibrated images given one vanishing point. In *Proc. of IEEE International Conference on Image Processing (ICIP)*, pages 361–364, 2005.
- [29] Murat Balci and Hassan Foroosh. Real-time 3d fire simulation using a spring-mass model. In *Proc. of Int. Multi-Media Modelling Conference*, pages 8–pp, 2006.
- [30] Murat Balci and Hassan Foroosh. Sub-pixel estimation of shifts directly in the fourier domain. *IEEE Trans. on Image Processing*, 15(7):1965–1972, 2006.
- [31] Murat Balci and Hassan Foroosh. Sub-pixel registration directly from phase difference. *Journal of Applied Signal Processing-special issue on Super-resolution Imaging*, 2006:1–11, 2006.
- [32] Herbert Bay, Tinne Tuytelaars, and Luc Van Gool. Surf: Speeded up robust features. In *European conference on computer vision*, pages 404–417. Springer, 2006.
- [33] M Berthod, M Werman, H Shekarforoush, and J Zerubia. Refining depth and luminance information using super-resolution. In *Proc. of IEEE Conf. Computer Vision and Pattern Recognition (CVPR)*, pages 654–657, 1994.
- [34] Marc Berthod, Hassan Shekarforoush, Michael Werman, and Josiane Zerubia. Reconstruction of high resolution 3d visual information. In *IEEE Conf. Computer Vision and Pattern Recognition (CVPR)*, pages 654–657, 1994.
- [35] Adeel Bhutta and Hassan Foroosh. Blind blur estimation using low rank approximation of cepstrum. *Image Analysis and Recognition*, pages 94–103, 2006.
- [36] Christopher M Bishop and Michael E Tipping. Bayesian image super resolution, September 12 2006. US Patent 7,106,914.
- [37] Francesca Bovolo, Lorenzo Bruzzone, Luca Capobianco, Andrea Garzelli, Silvia Marchesi, and Filippo Nencini. Analysis of the effects of pansharpening in change detection on vhr images. *IEEE Geoscience and Remote Sensing Letters*, 7(1):53–57, 2010.
- [38] Hakan Boyraz, Syed Zain Masood, Baoyuan Liu, Marshall Tappen, and Hassan Foroosh. Action recognition by weakly-supervised discriminative region localization.
- [39] Ozan Cakmakci, Gregory E. Fasshauer, Hassan Foroosh, Kevin P. Thompson, and Jannick P. Rolland. Meshfree approximation methods for free-form surface representation in optical design with applications to head-worn displays. In *Proc. SPIE Conf. on Novel Optical Systems Design and Optimization XI*, volume 7061, 2008.
- [40] Ozan Cakmakci, Brendan Moore, Hassan Foroosh, and Jannick Rolland. Optimal local shape description for rotationally non-symmetric optical surface design and analysis. *Optics Express*, 16(3):1583–1589, 2008.
- [41] Ozan Cakmakci, Sophie Vo, Hassan Foroosh, and Jannick Rolland. Application of radial basis functions to shape description in a dual-element off-axis magnifier. *Optics Letters*, 33(11):1237–1239, 2008.
- [42] X Cao and H Foroosh. Metrology from vertical objects. In *Proceedings of the British Machine Conference (BMVC)*, pages 74–1.
- [43] Xiaochun Cao and Hassan Foroosh. Camera calibration without metric information using 1d objects. In *Proc. International Conf. on Image Processing (ICIP)*, volume 2, pages 1349–1352, 2004.
- [44] Xiaochun Cao and Hassan Foroosh. Camera calibration without metric information using an isosceles trapezoid. In *Proc. International Conference on Pattern Recognition (ICPR)*, volume 1, pages 104–107, 2004.
- [45] Xiaochun Cao and Hassan Foroosh. Simple calibration without metric information using an isosceles trapezoid. In *Proc. of IAPR Int. Conf. Pattern Recognition (ICPR)*, volume 1, pages 104–107, 2004.
- [46] Xiaochun Cao and Hassan Foroosh. Camera calibration using symmetric objects. *IEEE Transactions on Image Processing*, 15(11):3614–3619, 2006.
- [47] Xiaochun Cao and Hassan Foroosh. Synthesizing reflections of inserted objects. In *Proc. IAPR Int. Conference on Pattern Recognition*, volume 2, pages 1225–1228, 2006.
- [48] Xiaochun Cao and Hassan Foroosh. Camera calibration and light source orientation from solar shadows. *Journal of Computer Vision & Image Understanding (CVIU)*, 105:60–72, 2007.
- [49] Xiaochun Cao, Wenqi Ren, Wangmeng Zuo, Xiaojie Guo, and Hassan Foroosh. Scene text deblurring using text-specific multi-scale dictionaries. *IEEE Transactions on Image Processing*, 24(4):1302–1314, 2015.
- [50] Xiaochun Cao, Yuping Shen, Mubarak Shah, and Hassan Foroosh. Single view compositing with shadows. *The Visual Computer*, 21(8-10):639–648, 2005.
- [51] Xiaochun Cao, Lin Wu, Jiangjian Xiao, Hassan Foroosh, Jigui Zhu, and Xiaohong Li. Video synchronization and its application on object transfer. *Image and Vision Computing (IVC)*, 28(1):92–100, 2009.

- [52] Xiaochun Cao, Jiangjian Xiao, and Hassan Foroosh. Camera motion quantification and alignment. In *Proc. International Conference on Pattern Recognition (ICPR)*, volume 2, pages 13–16, 2006.
- [53] Xiaochun Cao, Jiangjian Xiao, and Hassan Foroosh. Self-calibration using constant camera motion. In *Proc. of IAPR Int. Conf. Pattern Recognition (ICPR)*, volume 1, pages 595–598, 2006.
- [54] Xiaochun Cao, Jiangjian Xiao, Hassan Foroosh, and Mubarak Shah. Self-calibration from turn table sequence in presence of zoom and focus. *Computer Vision and Image Understanding (CVIU)*, 102(3):227–237, 2006.
- [55] Raymond H Chan, Tony F Chan, Lixin Shen, and Zuowei Shen. Wavelet algorithms for high-resolution image reconstruction. *SIAM Journal on Scientific Computing*, 24(4):1408–1432, 2003.
- [56] Kristian L Damkjær and Hassan Foroosh. Mesh-free sparse representation of multidimensional LIDAR data. In *Proc. of International Conference on Image Processing (ICIP)*, pages 4682–4686, 2014.
- [57] Hasan Demirel and Gholamreza Anbarjafari. Discrete wavelet transform-based satellite image resolution enhancement. *IEEE transactions on geoscience and remote sensing*, 49(6):1997–2004, 2011.
- [58] Weisheng Dong, D Zhang, Guangming Shi, and Xiaolin Wu. Image deblurring and super-resolution by adaptive sparse domain selection and adaptive regularization. *Image Processing, IEEE Transactions on*, 20(7):1838–1857, 2011.
- [59] Farshideh Einsele and Hassan Foroosh. Recognition of grocery products in images captured by cellular phones. In *Proc. International Conference on Computer Vision and Image Processing (ICCVIP)*, 2015.
- [60] Michael Elad and Yacov Hel-Or. A fast super-resolution reconstruction algorithm for pure translational motion and common space-invariant blur. *Image Processing, IEEE Transactions on*, 10(8):1187–1193, 2001.
- [61] G. Evangelidis. Iat: A matlab toolbox for image alignment. <http://www.iatool.net>, 2013.
- [62] Sina Farsiu, Michael Elad, and Peyman Milanfar. Multiframe demosaicing and super-resolution of color images. *Image Processing, IEEE Transactions on*, 15(1):141–159, 2006.
- [63] Martin A Fischler and Robert C Bolles. Random sample consensus: a paradigm for model fitting with applications to image analysis and automated cartography. *Communications of the ACM*, 24(6):381–395, 1981.
- [64] H Foroosh. Adaptive estimation of motion using generalized cross validation. In *3rd International (IEEE) Workshop on Statistical and Computational Theories of Vision*, 2003.
- [65] Hassan Foroosh. A closed-form solution for optical flow by imposing temporal constraints. In *Proc. of IEEE International Conf. on Image Processing (ICIP)*, volume 3, pages 656–659, 2001.
- [66] Hassan Foroosh. An adaptive scheme for estimating motion. In *Proc. of IEEE International Conf. on Image Processing (ICIP)*, volume 3, pages 1831–1834, 2004.
- [67] Hassan Foroosh. Pixelwise adaptive dense optical flow assuming non-stationary statistics. *IEEE Trans. on Image Processing*, 14(2):222–230, 2005.
- [68] Hassan Foroosh and Murat Balci. Sub-pixel registration and estimation of local shifts directly in the fourier domain. In *Proc. International Conference on Image Processing (ICIP)*, volume 3, pages 1915–1918, 2004.
- [69] Hassan Foroosh and Murat Balci. Subpixel registration and estimation of local shifts directly in the fourier domain. In *Proc. of IEEE International Conference on Image Processing (ICIP)*, volume 3, pages 1915–1918, 2004.
- [70] Hassan Foroosh, Murat Balci, and Xiaochun Cao. Self-calibrated reconstruction of partially viewed symmetric objects. In *Proc. IEEE Int. Conf. on Acoustics, Speech, and Signal Processing (ICASSP)*, volume 2, pages ii–869, 2005.
- [71] Hassan Foroosh and W Scott Hoge. Motion information in the phase domain. In *Video registration*, pages 36–71. Springer, 2003.
- [72] Hassan Foroosh, Josiane Zerubia, and Marc Berthod. Extension of phase correlation to subpixel registration. *IEEE Trans. on Image Processing*, 11(3):188–200, 2002.
- [73] William T Freeman, Thouis R Jones, and Egon C Pasztor. Example-based super-resolution. *Computer Graphics and Applications, IEEE*, 22(2):56–65, 2002.
- [74] Tao Fu and Hassan Foroosh. Expression morphing from distant viewpoints. In *Proc. of IEEE International Conference on Image Processing (ICIP)*, volume 5, pages 3519–3522, 2004.
- [75] Prakash P. Gajjar and Manjunath V. Joshi. New learning based super-resolution: Use of DWT and IGMRF prior. *IEEE Trans. Image Processing*, 19(5):1201–1213, 2010.
- [76] Daniel Glasner, Shai Bagon, and Michal Irani. Super-resolution from a single image. In *Computer Vision, 2009 IEEE 12th International Conference on*, pages 349–356. IEEE, 2009.
- [77] Michal Irani and Shmuel Peleg. Improving resolution by image registration. *CVGIP*, 53(3):231–239, 1991.
- [78] Apurva Jain, Supraja Murali, Nicolene Papp, Kevin Thompson, Kye-sung Lee, Panomsak Meemon, Hassan Foroosh, and Jannick P Rolland. Super-resolution imaging combining the design of an optical coherence microscope objective with liquid-lens based dynamic focusing capability and computational methods. In *Optical Engineering & Applications*, pages 70610C–70610C. International Society for Optics and Photonics, 2008.
- [79] Hui Ji and Cornelia Fermüller. Robust wavelet-based super-resolution reconstruction: theory and algorithm. *Pattern Analysis and Machine Intelligence, IEEE Transactions on*, 31(4):649–660, 2009.
- [80] CV Jiji, Manjunath V Joshi, and Subhasis Chaudhuri. Single-frame image super-resolution using learned wavelet coefficients. *International journal of Imaging systems and Technology*, 14(3):105–112, 2004.
- [81] Imran Junejo, Xiaochun Cao, and Hassan Foroosh. Configuring mixed reality environment. In *Proc. of IEEE International Conference on Advanced Video and Signal-based Surveillance*, pages 884–887, 2006.
- [82] Imran Junejo, Xiaochun Cao, and Hassan Foroosh. Geometry of a non-overlapping multi-camera network. In *Proc. of IEEE International Conference on Advanced Video and Signal-based Surveillance*, pages 43–48, 2006.
- [83] Imran Junejo, Xiaochun Cao, and Hassan Foroosh. Autoconfiguration of a dynamic non-overlapping camera network. *IEEE Trans. Systems, Man, and Cybernetics*, 37(4):803–816, 2007.
- [84] Imran Junejo and Hassan Foroosh. Dissecting the image of the absolute conic. In *Proc. of IEEE Int. Conf. on Video and Signal Based Surveillance*, pages 77–77, 2006.
- [85] Imran Junejo and Hassan Foroosh. Robust auto-calibration from pedestrians. In *Proc. IEEE International Conference on Video and Signal Based Surveillance*, pages 92–92, 2006.
- [86] Imran Junejo and Hassan Foroosh. Euclidean path modeling from ground and aerial views. In *Proc. International Conference on Computer Vision (ICCV)*, pages 1–7, 2007.
- [87] Imran Junejo and Hassan Foroosh. Trajectory rectification and path modeling for surveillance. In *Proc. International Conference on Computer Vision (ICCV)*, pages 1–7, 2007.
- [88] Imran Junejo and Hassan Foroosh. Using calibrated camera for euclidean path modeling. In *Proceedings of IEEE International Conference on Image Processing (ICIP)*, pages 205–208, 2007.
- [89] Imran Junejo and Hassan Foroosh. Euclidean path modeling for video surveillance. *Image and Vision Computing (IVC)*, 26(4):512–528, 2008.
- [90] Imran Junejo and Hassan Foroosh. Camera calibration and geo-location estimation from two shadow trajectories. *Computer Vision and Image Understanding (CVIU)*, 114(9):915–927, 2010.
- [91] Imran Junejo and Hassan Foroosh. Gps coordinates estimation and camera calibration from solar shadows. *Computer Vision and Image Understanding (CVIU)*, 114(9):991–1003, 2010.
- [92] Imran Junejo and Hassan Foroosh. Optimizing ptz camera calibration from two images. *Machine Vision and Applications (MVA)*, pages 1–15, 2011.

- [93] Imran N Junejo, Nazim Ashraf, Yuping Shen, and Hassan Foroosh. Robust auto-calibration using fundamental matrices induced by pedestrians. In *Proc. International Conf. on Image Processing (ICIP)*, volume 3, pages III–201, 2007.
- [94] Imran N Junejo, Xiaochun Cao, and Hassan Foroosh. Calibrating freely moving cameras. In *Proc. International Conference on Pattern Recognition (ICPR)*, volume 4, pages 880–883, 2006.
- [95] Imran N. Junejo and Hassan Foroosh. Trajectory rectification and path modeling for video surveillance. In *Proc. International Conference on Computer Vision (ICCV)*, pages 1–7, 2007.
- [96] Imran N. Junejo and Hassan Foroosh. Estimating geo-temporal location of stationary cameras using shadow trajectories. In *Proc. European Conference on Computer Vision (ECCV)*, 2008.
- [97] Imran N. Junejo and Hassan Foroosh. Gps coordinate estimation from calibrated cameras. In *Proc. International Conference on Pattern Recognition (ICPR)*, 2008.
- [98] Imran N Junejo and Hassan Foroosh. Gps coordinate estimation from calibrated cameras. In *Proc. International Conference on Pattern Recognition (ICPR)*, pages 1–4, 2008.
- [99] Imran N. Junejo and Hassan Foroosh. Practical ptz camera calibration using givens rotations. In *Proc. IEEE International Conference on Image Processing (ICIP)*, 2008.
- [100] Imran N. Junejo and Hassan Foroosh. Practical pure pan and pure tilt camera calibration. In *Proc. International Conference on Pattern Recognition (ICPR)*, 2008.
- [101] Imran N. Junejo and Hassan Foroosh. Refining ptz camera calibration. In *Proc. International Conference on Pattern Recognition (ICPR)*, 2008.
- [102] Imran N. Junejo and Hassan Foroosh. Using solar shadow trajectories for camera calibration. In *Proc. IEEE International Conference on Image Processing (ICIP)*, 2008.
- [103] Yonghyun Kim, Changno Lee, Dongyeob Han, Yongil Kim, and Younsoo Kim. Improved additive-wavelet image fusion. *IEEE Geoscience and Remote Sensing Letters*, 8(2):263–267, 2011.
- [104] Feng Li, Xiuping Jia, and Donald Fraser. Superresolution reconstruction of multispectral data for improved image classification. *IEEE Geoscience and Remote Sensing Letters*, 6(4):689–693, 2009.
- [105] Anne Lorette, Hassan Shekarforoush, and Josiane Zerubia. Super-resolution with adaptive regularization. In *Proc. International Conf. on Image Processing (ICIP)*, volume 1, pages 169–172, 1997.
- [106] Sina Lotfian and Hassan Foroosh. View-invariant object recognition using homography constraints. In *Proc. IEEE International Conference on Image Processing (ICIP)*, 2017.
- [107] Fei Lu, Xiaochun Cao, Yuping Shen, and Hassan Foroosh. Camera calibration from two shadow trajectories. In *Proc. of IEEE International Conference on Advanced Video and Signal-based Surveillance*, volume 2.
- [108] Antonio Marquina and Stanley J Osher. Image super-resolution by tv-regularization and bregman iteration. *Journal of Scientific Computing*, 37(3):367–382, 2008.
- [109] Brian Milikan, Aritra Dutta, Qiyu Sun, and Hassan Foroosh. Compressed infrared target detection using stochastically trained least squares. *IEEE Transactions on Aerospace and Electronics Systems*, page accepted, 2017.
- [110] Brian Millikan, Aritra Dutta, Nazanin Rahnavard, Qiyu Sun, and Hassan Foroosh. Initialized iterative reweighted least squares for automatic target recognition. In *Military Communications Conference, MILCOM, IEEE*, pages 506–510, 2015.
- [111] Brian A. Millikan, Aritra Dutta, Nazanin Rahnavard, Qiyu Sun, and Hassan Foroosh. Initialized iterative reweighted least squares for automatic target recognition. In *Proc. of MILCOM*, 2015.
- [112] Brendan Moore, Marshall Tappen, and Hassan Foroosh. Learning face appearance under different lighting conditions. In *Proc. IEEE Int. Conf. on Biometrics: Theory, Applications and Systems*, pages 1–8, 2008.
- [113] Dustin Morley and Hassan Foroosh. Improving ransac-based segmentation through cnn encapsulation. In *Proc. IEEE Conf. on Computer Vision and Pattern Recognition (CVPR)*, 2017.
- [114] Nhat Nguyen and Peyman Milanfar. An efficient wavelet-based algorithm for image superresolution. In *ICIP*, volume 2, pages 351–354. IEEE, 2000.
- [115] Xavier Otazu, María González-Audiciana, Octavi Fors, and Jorge Núñez. Introduction of sensor spectral response into image fusion methods. application to wavelet-based methods. *IEEE Transactions on Geoscience and Remote Sensing*, 43(10):2376–2385, 2005.
- [116] Rakesh C Patel and Manjunath V Joshi. Super-resolution of hyperspectral images: Use of optimum wavelet filter coefficients and sparsity regularization. *IEEE Transactions on Geoscience and Remote Sensing*, 53(4):1728–1736, 2015.
- [117] T. Ranchin and L. Wald. Comparison of different algorithms for the improvement of the spatial resolution of images. *Proc. 24th EARSeL Symposium Fusion of Earth Data: Merging Point Measurements, Raster Maps and Remotely Sensed Image*, 2000.
- [118] M Dirk Robinson, Cynthia A Toth, Joseph Y Lo, and Sina Farsiu. Efficient fourier-wavelet super-resolution. *Image Processing, IEEE Transactions on*, 19(10):2669–2681, 2010.
- [119] H Shekarforoush. *Super-Resolution in Computer Vision*. PhD thesis, PhD Thesis, University of Nice, 1996.
- [120] H Shekarforoush, M Berthod, and J Zerubia. Sub-pixel reconstruction of a variable albedo lambertian surface. In *Proceedings of the British Machine Vision Conference (BMVC)*, volume 1, pages 307–316.
- [121] H Shekarforoush and R Chellappa. adaptive super-resolution for predator video sequences.
- [122] H Shekarforoush and R Chellappa. A multifractal formalism for stabilization and activity detection in flir sequences. In *Proceedings, ARL Federated Laboratory 4th Annual Symposium*, pages 305–309, 2000.
- [123] H Shekarforoush, R Chellappa, H Niemann, H Seidel, and B Girod. Multi-channel superresolution for images sequences with applications to airborne video data. *Proc. of IEEE Image and Multidimensional Digital Signal Processing*, pages 207–210, 1998.
- [124] Hassan Shekarforoush. *Conditioning bounds for multi-frame super-resolution algorithms*. Computer Vision Laboratory, Center for Automation Research, University of Maryland, 1999.
- [125] Hassan Shekarforoush. Noise suppression by removing singularities. *IEEE Trans. Signal Processing*, 48(7):2175–2179, 2000.
- [126] Hassan Shekarforoush. Noise suppression by removing singularities. *IEEE transactions on signal processing*, 48(7):2175–2179, 2000.
- [127] Hassan Shekarforoush, Amit Banerjee, and Rama Chellappa. Super resolution for fopen sar data. In *Proc. AeroSense*, pages 123–129. International Society for Optics and Photonics, 1999.
- [128] Hassan Shekarforoush, Marc Berthod, Michael Werman, and Josiane Zerubia. Subpixel bayesian estimation of albedo and height. *International Journal of Computer Vision*, 19(3):289–300, 1996.
- [129] Hassan Shekarforoush, Marc Berthod, and Josiane Zerubia. 3d super-resolution using generalized sampling expansion. In *Proc. International Conf. on Image Processing (ICIP)*, volume 2, pages 300–303, 1995.
- [130] Hassan Shekarforoush, Marc Berthod, and Josiane Zerubia. *Subpixel image registration by estimating the polyphase decomposition of the cross power spectrum*. PhD thesis, INRIA-Technical Report, 1995.
- [131] Hassan Shekarforoush, Marc Berthod, and Josiane Zerubia. Subpixel image registration by estimating the polyphase decomposition of cross power spectrum. In *Proc. IEEE Conf. Computer Vision and Pattern Recognition (CVPR)*, pages 532–537, 1996.
- [132] Hassan Shekarforoush and Rama Chellappa. Blind estimation of psf for out of focus video data. In *Image Processing, 1998. ICIP 98. Proceedings. 1998 International Conference on*, pages 742–745, 1998.
- [133] Hassan Shekarforoush and Rama Chellappa. Data-driven multi-channel super-resolution with application to video sequences. *Journal of Optical Society of America-A*, 16(3):481–492, 1999.

- [134] Hassan Shekarforoush and Rama Chellappa. A multi-fractal formalism for stabilization, object detection and tracking in flir sequences. In *Proc. of International Conference on Image Processing (ICIP)*, volume 3, pages 78–81, 2000.
- [135] Hassan Shekarforoush, Josiane Zerubia, and Marc Berthod. Denoising by extracting fractional order singularities. In *Proc. of IEEE International Conf. on Acoustics, Speech and Signal Processing (ICASSP)*, volume 5, pages 2889–2892, 1998.
- [136] Huanfeng Shen, Liangpei Zhang, Bo Huang, and Pingxiang Li. A map approach for joint motion estimation, segmentation, and super resolution. *IEEE Transactions on Image processing*, 16(2):479–490, 2007.
- [137] Yuping Shen, Nazim Ashraf, and Hassan Foroosh. Action recognition based on homography constraints. In *Proc. of IAPR Int. Conf. Pattern Recognition (ICPR)*, pages 1–4, 2008.
- [138] Yuping Shen and Hassan Foroosh. View-invariant action recognition using fundamental ratios. In *Proc. IEEE Conference on Computer Vision and Pattern Recognition (CVPR)*, pages 1–6, 2008.
- [139] Yuping Shen and Hassan Foroosh. View invariant action recognition using fundamental ratios. In *Proc. IEEE Conference on Computer Vision and Pattern Recognition (CVPR)*, 2008.
- [140] Yuping Shen and Hassan Foroosh. View-invariant recognition of body pose from space-time templates. In *Proc. of IEEE Conf. on Computer Vision and Pattern Recognition*, pages 1–6, 2008.
- [141] Yuping Shen and Hassan Foroosh. View invariant recognition of body pose from space-time templates. In *Proc. IEEE Conference on Computer Vision and Pattern Recognition (CVPR)*, 2008.
- [142] Yuping Shen and Hassan Foroosh. View-invariant action recognition from point triplets. *IEEE Transactions on Pattern Analysis and Machine Intelligence (PAMI)*, 31(10):1898–1905, 2009.
- [143] Yuping Shen, Fei Lu, Xiaochun Cao, and Hassan Foroosh. Video completion for perspective camera under constrained motion. In *Proc. of IAPR Int. Conf. Pattern Recognition (ICPR)*, volume 3, pages 63–66, 2006.
- [144] Chen Shu, Luming Liang, Wenzhang Liang, and Hassan Foroosh. 3d pose tracking with multitemplate warping and sift correspondences. *IEEE Trans. on Circuits and Systems for Video Technology*, 26(11):2043–2055, 2016.
- [145] Chuan Sun and Hassan Foroosh. Should we discard sparse or incomplete videos? In *Proceedings of IEEE International Conference on Image Processing (ICIP)*, pages 2502–2506, 2014.
- [146] Chuan Sun, Imran Junejo, and Hassan Foroosh. Action recognition using rank-1 approximation of joint self-similarity volume. In *Proc. IEEE International Conference on Computer Vision (ICCV)*, pages 1007–1012, 2011.
- [147] Chuan Sun, Imran Junejo, and Hassan Foroosh. Motion retrieval using low-rank subspace decomposition of motion volume. In *Computer Graphics Forum*, volume 30, pages 1953–1962. Wiley, 2011.
- [148] Chuan Sun, Imran Junejo, and Hassan Foroosh. Motion sequence volume based retrieval for 3d captured data. *Computer Graphics Forum*, 30(7):1953–1962, 2012.
- [149] Chuan Sun, Imran Junejo, Marshall Tappen, and Hassan Foroosh. Exploring sparseness and self-similarity for action recognition. *IEEE Transactions on Image Processing*, 24(8):2488–2501, 2015.
- [150] Chuan Sun, Marshall Tappen, and Hassan Foroosh. Feature-independent action spotting without human localization, segmentation or frame-wise tracking. In *Proc. of IEEE Conference on Computer Vision and Pattern Recognition (CVPR)*, pages 2689–2696, 2014.
- [151] Amara Tariq and Hassan Foroosh. Scene-based automatic image annotation. In *Proc. of IEEE International Conference on Image Processing (ICIP)*, pages 3047–3051, 2014.
- [152] Amara Tariq and Hassan Foroosh. Feature-independent context estimation for automatic image annotation. In *Proceedings of the IEEE Conference on Computer Vision and Pattern Recognition (CVPR)*, pages 1958–1965, 2015.
- [153] Amara Tariq and Hassan Foroosh. T-clustering: Image clustering by tensor decomposition. In *Proc. of International Conference on Image Processing (ICIP)*, pages 4803–4807, 2015.
- [154] Amara Tariq, Asim Karim, and Hassan Foroosh. A context-driven extractive framework for generating realistic image descriptions. *IEEE Transactions on Image Processing*, 26(2):619–632, 2002.
- [155] Amara Tariq, Asim Karim, and Hassan Foroosh. Nelasso: Building named entity relationship networks using sparse structured learning. *IEEE Trans. on Pattern Analysis and Machine Intelligence*, 2017.
- [156] Amara Tariq, Asim Karim, Fernando Gomez, and Hassan Foroosh. Exploiting topical perceptions over multi-lingual text for hashtag suggestion on twitter. In *The Twenty-Sixth International FLAIRS Conference*, 2013.
- [157] A Temizel and T Vlachos. Wavelet domain image resolution enhancement using cycle-spinning. *Electronics Letters*, 41(3):119–121, 2005.
- [158] Jing Tian and Kai-Kuang Ma. A survey on super-resolution imaging. *Signal, Image and Video Processing*, 5(3):329–342, 2011.
- [159] RY Tsai and Thomas S Huang. Multiframe image restoration and registration. *Advances in computer vision and Image Processing*, 1(2):317–339, 1984.
- [160] Patrick Vandewalle, Luciano Sbaiz, Joos Vandewalle, and Martin Vetterli. Super-resolution from unregistered and totally aliased signals using subspace methods. *Signal Processing, IEEE Transactions on*, 55(7):3687–3703, 2007.
- [161] Zhangyang Wang, Yingzhen Yang, Zhaowen Wang, Shiyu Chang, Wei Han, Jianchao Yang, and Thomas Huang. Self-tuned deep super resolution. In *Proceedings of the IEEE Conference on Computer Vision and Pattern Recognition Workshops*, pages 1–8, 2015.
- [162] Jiangjian Xiao, Xiaochun Cao, and Hassan Foroosh. 3d object transfer between non-overlapping videos. In *Proc. of IEEE Virtual Reality Conference*, pages 127–134, 2006.
- [163] Jiangjian Xiao, Xiaochun Cao, and Hassan Foroosh. A new framework for video cut and paste. In *Proc. of Int. Conf. on Multi-Media Modelling Conference Proceedings*, pages 8–pp, 2006.
- [164] Changqing Zhang, Xiaochun Cao, and Hassan Foroosh. Constrained multi-view video face clustering. *IEEE Transactions on Image Processing*, 24(11):4381–4393, 2015.
- [165] Hongyan Zhang, Liangpei Zhang, and Huanfeng Shen. A super-resolution reconstruction algorithm for hyperspectral images. *Signal Processing*, 92(9):2082–2096, 2012.
- [166] Kaibing Zhang, Xinbo Gao, Xuelong Li, and Dacheng Tao. Partially supervised neighbor embedding for example-based image super-resolution. *Selected Topics in Signal Processing, IEEE Journal of*, 5(2):230–239, 2011.
- [167] Shubin Zhao, Hua Han, and Silong Peng. Wavelet-domain hmt-based image super-resolution. In *Proceedings of the 2003 International Conference on Image Processing (ICIP)*, pages 953–956, 2003.
- [168] Fei Zhou, Wenming Yang, and Qingmin Liao. Interpolation-based image super-resolution using multisurface fitting. *Image Processing, IEEE Transactions on*, 21(7):3312–3318, 2012.
- [169] J. Zhou, D. L. Civco, and J. A. Silander. A wavelet transform method to merge landsat tm and spot panchromatic data. *International Journal of Remote Sensing*, 19(4):743–757, 1998.